Achromatopsia mutations target sequential steps of ATF6 activation

Wei-Chieh Chiang[a], Priscilla Chan[a], Bernd Wissinger[b], Ajoy Vincent[c], Anna Skorczyk-Werner[d], Maciej R. Krawczyński[d,e], Randal J. Kaufman[f], Stephen H. Tsang[g,h,i], Elise Héon[c], Susanne Kohl[b], and Jonathan H. Lin[a,j,1]

[a]Department of Pathology, University of California, San Diego, La Jolla, CA 92093; [b]Institute for Ophthalmic Research, University of Tubingen, D-72076 Tubingen, Germany; [c]Department of Ophthalmology and Vision Sciences, University of Toronto, Toronto, ON, Canada M5T 3A9; [d]Department of Medical Genetics, Poznan University of Medical Sciences, 60-806, Poznan, Poland; [e]Center for Medical Genetics GENESIS, 60-601, Poznan, Poland; [f]Degenerative Diseases Program, Sanford-Burnham-Prebys Medical Discovery Institute, La Jolla, CA 92037; [g]Jonas Children's Vision Care and Bernard & Shirlee Brown Glaucoma Laboratory, Irving Comprehensive Cancer Center, Columbia University, New York, NY 10032; [h]Edward S. Harkness Eye Institute, New York-Presbyterian Hospital, New York, NY 10032; [i]Departments of Ophthalmology, Pathology & Cell Biology, Institute of Human Nutrition, College of Physicians and Surgeons, Columbia University, New York, NY 10032; and [j]VA San Diego Healthcare System, San Diego, CA 92161

Edited by Jonathan S. Weissman, University of California, San Francisco, CA, and approved November 30, 2016 (received for review April 21, 2016)

Achromatopsia is an autosomal recessive disorder characterized by cone photoreceptor dysfunction. We recently identified activating transcription factor 6 (*ATF6*) as a genetic cause of achromatopsia. ATF6 is a key regulator of the unfolded protein response. In response to endoplasmic reticulum (ER) stress, ATF6 migrates from the ER to Golgi to undergo regulated intramembrane proteolysis to release a cytosolic domain containing a basic leucine zipper (bZIP) transcriptional activator. The cleaved ATF6 fragment migrates to the nucleus to transcriptionally up-regulate protein-folding enzymes and chaperones. *ATF6* mutations in patients with achromatopsia include missense, nonsense, splice site, and single-nucleotide deletion or duplication changes found across the entire gene. Here, we comprehensively tested the function of achromatopsia-associated *ATF6* mutations and found that they group into three distinct molecular pathomechanisms: class 1 ATF6 mutants show impaired ER-to-Golgi trafficking and diminished regulated intramembrane proteolysis and transcriptional activity; class 2 ATF6 mutants bear the entire ATF6 cytosolic domain with fully intact transcriptional activity and constitutive induction of downstream target genes, even in the absence of ER stress; and class 3 ATF6 mutants have complete loss of transcriptional activity because of absent or defective bZIP domains. Primary fibroblasts from patients with class 1 or class 3 *ATF6* mutations show increased cell death in response to ER stress. Our findings reveal that human *ATF6* mutations interrupt distinct sequential steps of the ATF6 activation mechanism. We suggest that increased susceptibility to ER stress-induced damage during retinal development underlies the pathology of achromatopsia in patients with *ATF6* mutations.

cone photoreceptor | achromatopsia | endoplasmic reticulum stress | ATF6 | unfolded protein response

Achromatopsia is a heritable blinding disease caused by cone photoreceptor dysfunction that spares the rod system. Using next-generation whole-exome sequencing, we recently discovered autosomal recessive mutations in the activating transcription factor 6 (*ATF6*) gene in patients with achromatopsia (1). *ATF6* mutations span the entire coding region and include missense, nonsense, splice site, and single-nucleotide deletion and duplication changes (1–3). We previously showed that a missense mutation that introduced an arginine-to-cysteine substitution at amino acid residue 324 of the ATF6 protein compromised ATF6 activity in patient fibroblasts obtained from an achromatopsia family (1). However, the functional consequences of the other *ATF6* mutations found in patients with achromatopsia remain unknown.

In humans, ATF6 is a 670-amino acid glycosylated transmembrane protein found in the endoplasmic reticulum (ER) (4). In response to protein misfolding in the ER or other forms of ER stress, ATF6 migrates from the ER to the Golgi apparatus, where the site 1 protease (S1P) and site 2 protease (S2P) cleave ATF6 in the transmembrane domain to liberate the cytosolic domain of ATF6 (4–6). The cytosolic domain contains a transcription factor of the basic leucine zipper (bZIP) family (4). Upon release from the Golgi membrane, the free ATF6 cytosolic transcriptional activator fragment migrates to the nucleus to bind DNA and transcriptionally up-regulate target genes that include ER protein folding chaperones and enzymes (4, 7, 8). Via this signal transduction mechanism, ATF6 activation helps restore ER protein folding homeostasis and alleviates ER stress (9).

Here, we investigated how *ATF6* mutations found in patients with achromatopsia affect ATF6's molecular mechanism of signaling and activation, using patient fibroblasts and recombinant mutant ATF6 proteins. We identified a class of *ATF6* mutations in the luminal domain that reduce ATF6 signaling by impairing ER-to-Golgi trafficking of full-length ATF6 during ER stress. We identified a second class of *ATF6* mutations near the transmembrane domain that have the potential to produce intact ATF6 cytosolic fragments with fully functional transcriptional activator properties. Last, we identified a third class of *ATF6* mutations in the cytosolic domain that cause the loss of ATF6 function by deletion or mutation of the bZIP and/or transcriptional activator domain. Patient fibroblasts with loss-of-function *ATF6* mutations exhibited significantly increased cell death in response to ER stress.

Significance

The unfolded protein response regulator activating transcription factor 6 (*ATF6*) was recently identified as a novel genetic cause of the cone photoreceptor disease achromatopsia. ATF6 upregulates genes that help cells cope with endoplasmic reticulum stress. We identified the pathomechanisms of all *ATF6* achromatopsia mutations. Class 1 ATF6 mutants show impaired endoplasmic reticulum (ER)-to-Golgi trafficking and diminished production of the transcriptional activator fragment. Class 2 mutants encode the intact ATF6 transcriptional activator domain with full activity. Class 3 mutants have defective basic leucine zipper (bZIP) domains with abrogated function. Patient fibroblasts show increased apoptosis after ER stress. Our findings reveal that human *ATF6* mutations interrupt distinct steps of ATF6 activation. ER stress-associated damage may underlie the pathology of achromatopsia arising from *ATF6*.

Author contributions: W.-C.C. and J.H.L. designed research; W.-C.C., P.C., and J.H.L. performed research; W.-C.C., B.W., A.V., A.S.-W., M.R.K., R.J.K., S.H.T., E.H., S.K., and J.H.L. contributed new reagents/analytic tools; W.-C.C., B.W., A.V., A.S.-W., M.R.K., R.J.K., S.H.T., E.H., S.K., and J.H.L. analyzed data; and W.-C.C., S.K., and J.H.L. wrote the paper.

The authors declare no conflict of interest.

This article is a PNAS Direct Submission.

[1]To whom correspondence should be addressed. Email: JLin@ucsd.edu.

This article contains supporting information online at www.pnas.org/lookup/suppl/doi:10.1073/pnas.1606387114/-/DCSupplemental.

www.pnas.org/cgi/doi/10.1073/pnas.1606387114

Results

Class 1 ATF6[Y567N] Mutation Impairs ER-to-Golgi Trafficking During ER Stress. Four achromatopsia-associated ATF6 mutations introduce missense or frame shift changes in exons encoding the ER luminal domain of ATF6 (Fig. S1) (1, 3). We previously identified a family with a tyrosine-to-asparagine substitution at amino acid position 567 in the luminal domain of ATF6 (1). We obtained fibroblasts from two unaffected heterozygous ($ATF6^{Y567N/+}$) parents, probands 1 and 2, and a homozygous ($ATF6^{Y567N/Y567N}$) affected child, patient 3 (Fig. 1*A*). We found comparable levels of *ATF6* mRNA and full-length ATF6 protein in heterozygous and homozygous fibroblasts under standard cell culturing conditions (Fig. 1 *B* and *C*). During ER stress conditions experimentally induced by tunicamycin application, *ATF6* mRNA levels and the full-length ATF6 protein levels were up-regulated in both heterozygous and homozygous fibroblasts compared with the untreated samples (Fig. 1 *B* and *C*). However, significantly reduced levels of the cleaved ATF6 cytosolic fragment were seen in homozygous $ATF6^{Y567N/Y567N}$ fibroblasts compared with heterozygous controls in response to experimental ER stress induced by DTT (Fig. 1*D*). These findings showed that *ATF6* mRNA and full-length protein were normally generated in the $ATF6^{Y567N}$ mutant, but during ER stress, lower levels of the cleaved functional transcriptional activator domain of ATF6 were present in $ATF6^{Y567N/Y567N}$ fibroblasts despite normal to increased levels of full-length ATF6 protein compared with heterozygous controls. Consistent with reduction of the ATF6 transcriptionally active fragment, we found reduced levels of *BIP/GRP78* mRNA and protein, an ER chaperone transcriptionally up-regulated by ATF6 (4, 7, 10), in $ATF6^{Y567N/Y567N}$ fibroblasts compared with heterozygous controls in response to experimental ER stress (Fig. 1 *E* and *F*). These findings revealed that the luminal ATF6 [Y567N] mutation resulted in the impairment of ATF6 signaling in $ATF6^{Y567N/Y567N}$ fibroblasts during ER stress.

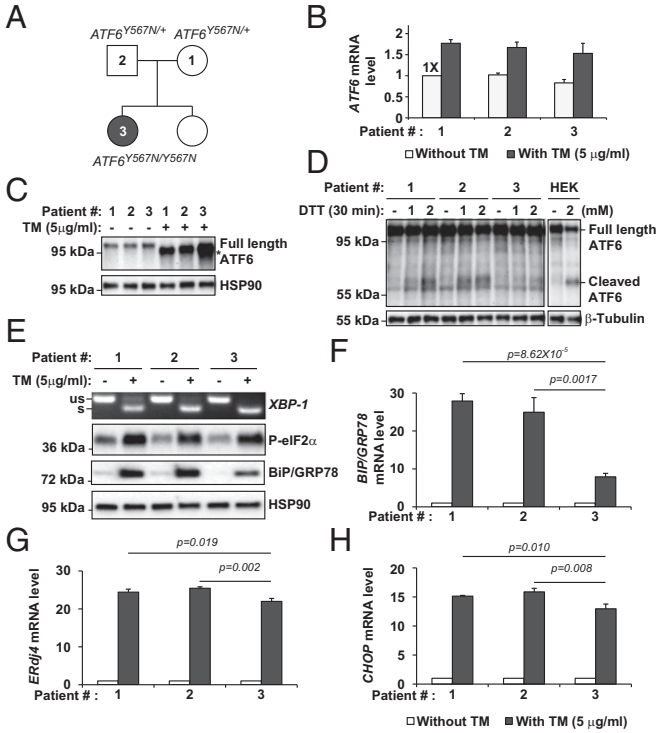

Fig. 1. Impaired cleavage of ATF6 in response to ER stress in class 1 mutant ATF6[Y567N] patient fibroblasts. (*A*) Pedigree of the family carrying $ATF6^{Y567N}$ alleles. The heterozygous parents ($ATF6^{Y567N/+}$) were indicated as patient 1 and 2 for the mother and the father, respectively. The homozygous ($ATF6^{Y567N/Y567N}$) female child was indicated as patient 3. (*B*) $ATF6^{Y567N/+}$ or $ATF6^{Y567N/Y567N}$ patient fibroblasts were challenged with tunicamycin (TM) at the indicated concentration for 24 h. mRNA was collected from the fibroblasts. *ATF6* mRNA levels were measured by real-time quantitative PCR and normalized to the level in the untreated $ATF6^{Y567N/+}$ parental control (patient #1) fibroblast cells. (*C*) Patient fibroblasts expressing ATF6[Y567N] were challenged with TM at the indicated concentration for 24 h. Endogenous ATF6 protein levels were detected by immunoblotting. *Position of the deglycosylated full-length ATF6 protein produced after TM treatment. (*D*) Patient fibroblasts expressing ATF6[Y567N] were challenged with DTT for 30 min, and ATF6 protein levels were detected by immunoblotting using anti-ATF6 antibody. To help identify the electrophoretic migration patterns of full-length and cleaved ATF6 fragments, HEK293 cells were also challenged with DTT, and lysates were immunoblotted with anti-ATF6 antibody. (*E*) Patient fibroblasts were challenged with TM at the indicated concentration for 24 h. *XBP1* mRNA splicing was assessed by RT-PCR. The level of phosphorylated-eIF2α and BiP/GRP78 were detected by immunoblotting. (*F–H*) The mRNA levels of ATF6 downstream target gene *BIP/GRP78* (*F*), IRE1 downstream target gene *ERdj4* (*G*), and PERK downstream target gene *CHOP* (*H*) were assessed by real-time quantitative PCR and normalized to mRNA levels in untreated samples.

ATF6 signaling is a key component of the unfolded protein response (UPR) and operates in parallel with UPR signal transduction pathways controlled by the inositol-requiring enzyme 1 (IRE1) and PKR-like endoplasmic reticulum kinase (PERK) proteins to ensure normal ER function in mammalian cells (11, 12). We next examined whether the other branches of the UPR were also dysregulated in $ATF6^{Y567N/Y567N}$ fibroblasts. We assayed two specific molecular events of the IRE1 UPR signaling pathway, *XBP1* mRNA splicing, an early proximal event specifically initiated by IRE1 activation (13, 14), and *ERdj4* transcription, a downstream target gene induced by IRE1 signaling (Fig. 1 *E* and *G*) (7, 8, 15, 16). For the UPR signaling pathway regulated by PERK, we examined levels of phosphorylated eIF2α protein, an early proximal event in the PERK signal transduction pathway (17, 18), and *CHOP* mRNA transcript, a downstream target gene potently up-regulated by PERK signaling (Fig. 1 *E* and *H*) (19). For these IRE1 and PERK pathway markers, we observed a small (<10%) but statistically significant decrease in *ERdj4* and *CHOP* transcript levels between $ATF6^{Y567N/Y567N}$ fibroblasts and heterozygous controls (Fig. 1 *E–H*). These studies revealed that $ATF6^{Y567N/Y567N}$ fibroblasts with compromised ATF6 signaling also showed mild impairment of the transcriptional output of other UPR pathways during ER stress.

Next, we investigated the mechanism underlying the reduction in levels of the cleaved ATF6 fragment observed during ER stress in $ATF6^{Y567N/Y567N}$ fibroblasts. To ensure that the ATF6 protein level differences were not a result of fibroblast cell line differences, we expressed FLAG-tagged full-length wild-type ATF6 or mutant ATF6[Y567N] in HEK293 cells. Similar to our findings in the primary patient fibroblasts, we observed significantly reduced levels of cleaved ATF6 in response to ER stress induced by DTT in cells expressing ATF6[Y567N] compared with wild-type ATF6 (Fig. 2*A*). In response to ER stress, full-length ATF6 traffics from ER to Golgi, where the Golgi-resident S1P and S2P proteases cleave the full-length protein to liberate the cytosolic transcriptional activator ATF6 fragment. We examined whether defects in ER-to-Golgi trafficking were responsible for the reduced production of cleaved ATF6 seen with the ATF6[Y567N] mutant. First, we compared the sensitivity with endoglycosidase H (Endo H) of wild-type ATF6 and the ATF6[Y567N] mutant. Prior studies had demonstrated that ATF6 was glycosylated with high mannose *N*-glycan in the ER and that this glycosylated ATF6 isoform was sensitive to Endo H (4, 5). When ATF6 traveled to Golgi during ER stress, the high mannose *N*-glycan of ATF6 was trimmed by glycosidases in the Golgi to produce an Endo H-resistant full-length ATF6 that could be transiently visualized by SDS/PAGE in cells before undergoing S1P protease cleavage (5).

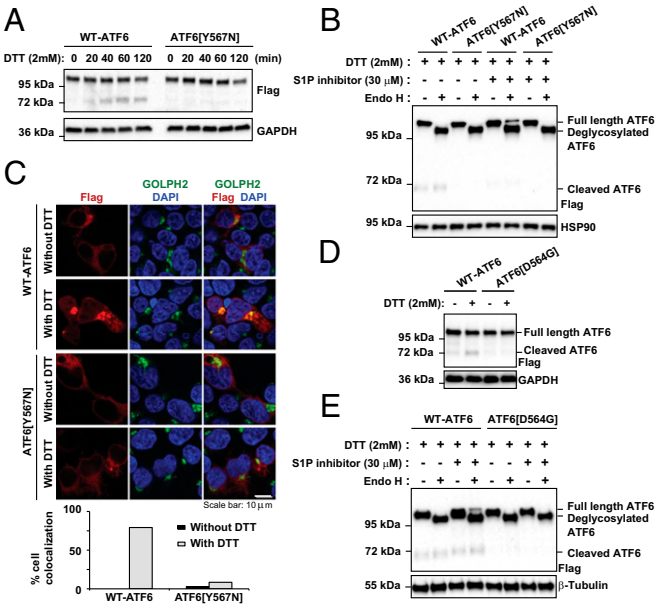

Fig. 2. Impaired ER-to-Golgi trafficking of class 1 mutants ATF6[Y567N] and ATF6[D564G] during ER stress. (*A*) Recombinant FLAG-tagged ATF6[Y567N] was expressed in HEK293 cells for 20 h and then challenged with DTT as indicated. ATF6 protein levels were detected by immunoblotting with anti-FLAG. The band above 95 kDa and the band at 72 kDa represent the full-length FLAG-tagged ATF6 and cleaved FLAG-tagged ATF6, respectively. (*B*) Recombinant FLAG-tagged wild-type ATF6 and ATF6[Y567N] were expressed in HEK293 cells for 20 h and then challenged with DTT with or without S1P inhibitor, as indicated, for 90 min. Cell lysates were treated with Endo H, as indicated. ATF6 protein levels were detected by immunoblotting with anti-FLAG. The bands above 95 kDa and the band at 72 kDa represent the full-length FLAG-tagged ATF6 (either Endo H sensitive or insensitive) and cleaved FLAG-tagged ATF6, respectively. (*C*) ATF6[Y567N] was expressed in HEK293 cells for 20 h and then challenged with 2 mM DTT for 40 min. The subcellular localization of ATF6 was visualized by immunofluorescence labeling and confocal microscopy by anti-FLAG antibody (shown in red). The Golgi apparatus was visualized by GOLPH2 immunostaining (shown in green). The nucleus was visualized by DAPI staining (shown in blue). The percentage of cells showing FLAG and GOLPH2 colocalization was quantified and shown in the bottom graph. (Scale bar, 10 μm.) (*D*) Recombinant FLAG-tagged ATF6[D564G] was expressed in HEK293 cells for 20 h and then challenged with DTT for 1 h. ATF6 protein levels were detected by immunoblotting with anti-FLAG. (*E*) Recombinant FLAG-tagged wild-type ATF6 and ATF6[D564G] were expressed in HEK293 cells for 20 h and then challenged with DTT with or without S1P inhibitor, as indicated, for 90 min. Cell lysates were treated with Endo H, as indicated.

We found that both wild-type ATF6 and the mutant ATF6[Y567N] underwent glycosylation in the ER and showed identical Endo H sensitivity profiles (Fig. 2*B*). However, when we added S1P inhibitor and analyzed protein lysates collected from cells treated with DTT, we saw an Endo H-resistant ATF6 isoform only with wild-type ATF6 (Fig. 2*B*). This finding provided biochemical evidence that the mutant ATF6[Y567N] trafficked poorly from ER to Golgi compared with the wild-type protein during ER stress. Consistent with these biochemical results, when we examined the subcellular localization of ATF6 by fluorescence confocal microscopy, we found colocalization of wild-type ATF6 and the Golgi marker Golgi membrane protein 1 (GOLPH2), in response to ER stress induced by DTT (Fig. 2*C*, *upper two rows*). However, the mutant ATF6[Y567N] and GOLPH2 remained in separate subcellular compartments with no colocalization of fluorescent signals under the same experimental conditions (Fig. 2*C*, *bottom two rows*). We confirmed that both wild-type and mutant ATF6[Y567N] were localized in the ER under resting (nonstressed) conditions, as evident by colocalization with the ER resident protein, PDI (Fig. S2). Another luminal domain mutant, ATF6[D564G], also showed impaired cleavage and trafficking in analogous assays (Fig. 2 *D* and *E*). In sum, our studies revealed that the mechanism underlying attenuation of transcriptional activity in class 1 ATF6 luminal domain mutants arose from an unexpected defect in the process of ER-to-Golgi trafficking in response to ER stress, leading to reduced production of the cleaved transcriptional activator domain of ATF6.

Constitutive Transcriptional Activity in Class 2 ATF6 Mutants. The amino terminal domain of ATF6 is a 370–380-amino acid bZIP transcription factor, and expression of recombinant ATF6 protein bearing only the first 373 amino acids from ATF6's cytosolic domain reconstituted the transcriptional activity of ATF6 in mammalian cells (4, 20). Intriguingly, three of the *ATF6* mutations identified in patients with achromatopsia were predicted to create ATF6 fragments of similar length to the ATF6(373) transcriptionally active fragment (Fig. S1 and refs. 1 and 3). To determine whether this group of *ATF6* mutations showed functional activity, we expressed a recombinant FLAG-tagged ATF6 bearing a frame-shift mutation that caused a valine-to-serine substitution at amino acid 371 of ATF6, followed by a stop codon three amino acids distally, ATF6[V371Sfs*3]. We found that the ATF6[V371Sfs*3] protein showed nearly identical size mobility to ATF6(373) in transfected HEK293 cells (Fig. 3*A*, compare lane 5 and lane 2). We also found that ATF6[V371Sfs*3] transcriptionally induced ATF6 downstream target genes, *BIP*/*GRP78*, *HERPUD1*, and *SEL1L*, as potently as ATF6(373) (21) (Fig. 3*B*). The expression of *CHOP* was also up-regulated by both ATF6(373) and ATF6[V371Sfs*3] (Fig. 3*B*). In analogous studies, we also found that the ATF6[R376*] mutant showed nearly identical size mobility to ATF6(373), and induction of ATF6 downstream target gene, BIP/GRP78 (Fig. S3). These findings demonstrated that the recombinant mutant ATF6 [V371Sfs*3] and ATF6[R376*] proteins are fully functional transcriptional activators in vitro. In vivo, the amount of functional truncated ATF6[V371Sfs*3] and ATF6[R376*] proteins may be less than wild-type ATF6 protein levels because the nonsense and premature stop codons found in these mutants may subject their mRNA transcripts to nonsense-mediated mRNA decay (NMD) (1).

Class 3 ATF6 Mutants Are Transcriptionally Inactive. Five *ATF6* mutations found in patients with achromatopsia introduce nonsense or premature stop codons in exons encoding the cytosolic domain of ATF6 and are predicted to produce ATF6 cytosolic protein fragments with nonfunctional bZIP or lacking the entire bZIP and transcriptional activator domains (Fig. S1 *B* and *C* and refs. 1 and 2). To test whether this group of *ATF6* mutations compromised ATF6 function, we expressed recombinant FLAG-tagged ATF6 bearing several of these mutations, including a proline-to-leucine mutation at position 118, followed by a premature stop codon 31 amino acids distally, ATF6[P118Lfs*31], which lacks the bZIP domain and part of the transcription activator domain, and a nonsense mutation of an asparagine residue at position 267, ATF6[N267*], which lacks only the bZIP domain. We detected protein expression of these truncated ATF6 mutants after transfection into HEK293 cells (Fig. 3*A*), but found no transcriptional induction of ATF6 target proteins with either mutant (Fig. 3 *A* and *B*). Coupled with our prior studies of the ATF6[R324C] mutant (1), these results identify a class of disease-associated *ATF6* mutations that cause loss of function through disruption of transcriptional activity by truncating the bZIP and/or transcriptional activator domains or by directly mutating critical residues in the bZIP domain in the ATF6 cytosolic domain.

To determine how the loss of ATF6 activity affected other signaling arms of the UPR in patient cells with this class of mutations, we examined fibroblasts previously collected from a family

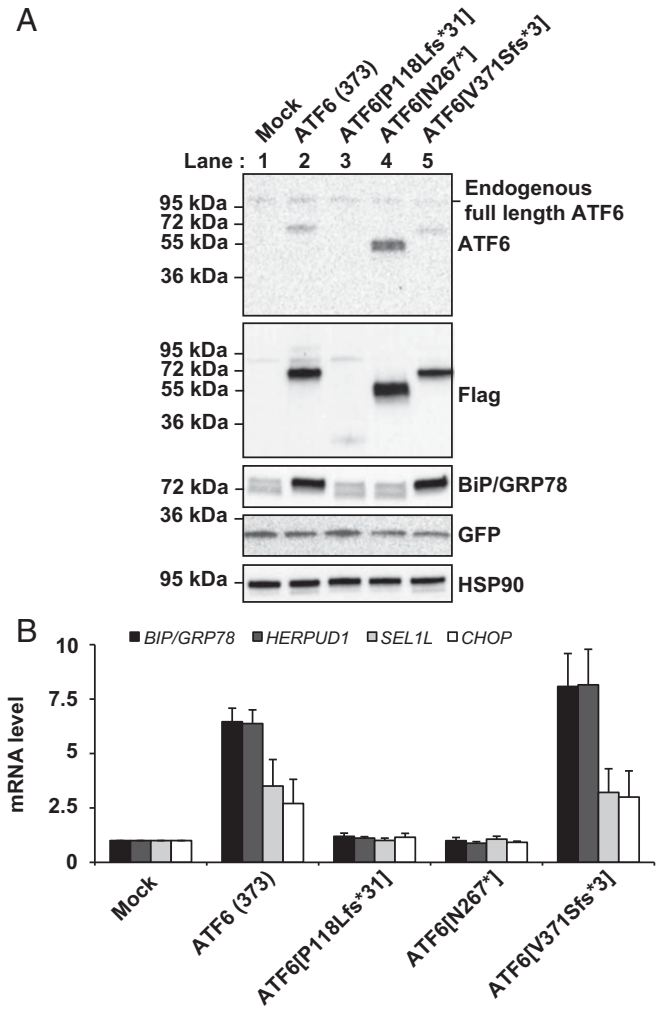

Fig. 3. Transcriptional activator properties of class 2 and class 3 mutant ATF6 proteins. (*A*) FLAG epitope-tagged ATF6(373), ATF6[V371Sfs*3] (a class 2 mutant), and ATF6[P118Lfs*31] and ATF6[N267*] (class 3 mutants) were cotransfected with GFP into HEK293 cells. ATF6 protein levels were detected by immunoblotting, using anti-ATF6 and anti-FLAG antibodies. BiP/GRP78 and GFP protein levels were detected by immunoblotting. GFP levels were assessed as a transfection control. (*B*) ATF6(373), ATF6[P118Lfs*31], ATF6 [N267*], and ATF6[V371Sfs*3] were expressed in the HEK293 cells and mRNA was collected. Levels of genes transcriptionally regulated by ATF6, including *BIP/GRP78, HERPUD1*, and *SEL1L*, were measured by real-time quantitative PCR and normalized to levels in mock transfected cells. *CHOP*, a gene that is regulated by PERK activation, was also assessed.

expressing the ATF6[R324C] mutation (1). These included an unaffected heterozygous parent ($ATF6^{R324C/+}$), proband 1, and three affected homozygous achromatic children ($ATF6^{R324C/R324C}$), patients 2, 3, and 4 (Fig. 4*A*). We found comparable levels of *ATF6* mRNA and full-length ATF6 protein in heterozygous and homozygous fibroblasts (Fig. 4 *B* and *C*). During experimentally induced ER stress conditions, we found increased levels of *ATF6* mRNA and protein in heterozygous and homozygous fibroblasts (Fig. 4 *B* and *C*). However, we found reduced levels of BiP/GRP78 protein in $ATF6^{R324C/R324C}$ fibroblasts compared with heterozygous controls in response to experimental ER stress consistent with our prior studies that showed that the ATF6[R324C] mutation compromised ATF6 signaling activity (Fig. 4*C*). This signaling defect arose from impairment of the bZIP transcriptional activator domain itself, and not at earlier steps in the trafficking or production of the cytosolic ATF6 fragment, because full-length ATF6[R324C] protein underwent ER-to-Golgi trafficking (Fig. 5 *B* and *C*) and produced the cleaved ATF6 transcriptional activator fragment with similar kinetics to the wild-type protein in response to ER stress (Fig. 5*A*).

We next examined whether the IRE1 and PERK signaling branches of the UPR were dysregulated in $ATF6^{R324C/R324C}$ fibroblasts. For IRE1 pathway markers, we saw no difference in *XBP1* mRNA levels or *XBP1* mRNA splicing between $ATF6^{R324C/R324C}$ fibroblasts and heterozygous control (Fig. 4*D* and Fig. S4). However, we saw significantly reduced transcriptional induction of *ERdj4* in $ATF6^{R324C/R324C}$ fibroblasts compared with heterozygous control (Fig. 4 *D* and *E*). For the PERK pathway markers, we saw no difference in eIF2α phosphorylation between $ATF6^{R324C/R324C}$ fibroblasts and heterozygous control (Fig. 4*C*). However, we saw significantly reduced transcriptional induction of *CHOP* in $ATF6^{R324C/R324C}$ fibroblasts compared with heterozygous control (Fig. 4 *C* and *F*). These studies revealed that $ATF6^{R324C/R324C}$ fibroblasts show compromised ATF6 transcriptional activity as well as significant impairment of the transcriptional output from the IRE1 and PERK signaling branches of the UPR during ER stress.

Class 1 and Class 3 ATF6 Mutant Fibroblasts Are More Susceptible to ER Stress-Mediated Cell Death. Our studies revealed that class 1 and class 3 *ATF6* mutations both impaired ATF6 function. ATF6 ameliorates ER stress through its transcriptional induction of ER

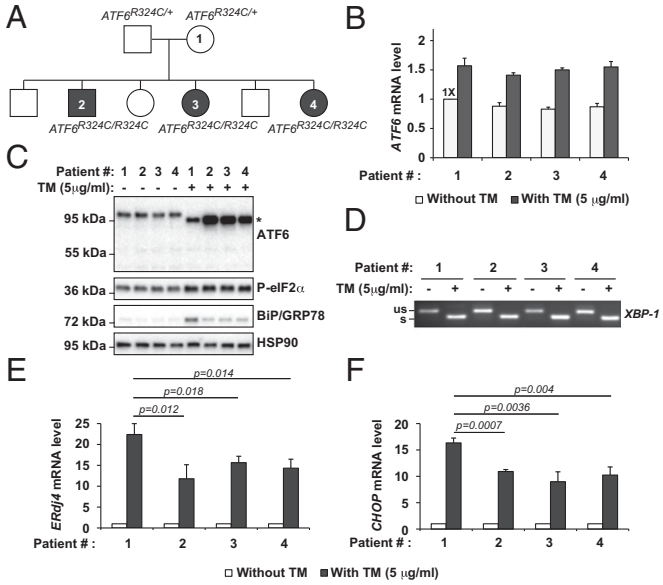

Fig. 4. ATF6, IRE1, and PERK activity in class 3 mutant, $ATF6^{R324C}$, patient fibroblasts. (*A*) Pedigree of the family carrying $ATF6^{R324C}$ alleles. The heterozygous mother ($ATF6^{R324C/+}$) was indicated as patient 1. The homozygous ($ATF6^{R324C/R324C}$) children were indicated as patients 2, 3, and 4. (*B*) $ATF6^{R324C/+}$ or $ATF6^{R324C/R324C}$ patient fibroblasts were challenged with TM at the indicated concentration for 24 h. mRNA was collected from the fibroblasts. *ATF6* mRNA levels were measured by real-time quantitative PCR and normalized to the level in the untreated $ATF6^{R324C/+}$ parental control (patient #1) fibroblast cells. (*C*) $ATF6^{R324C/+}$ or $ATF6^{R324C/R324C}$ patient fibroblasts were challenged with TM for 24 h. ATF6, phosphorylated-eIF2α, and BiP/GRP78 were detected in protein lysates by immunoblotting. *Position of the deglycosylated full-length ATF6 protein produced after TM treatment. (*D*) *XBP1* mRNA splicing was visualized by semiquantitative RT-PCR from patient fibroblasts treated with TM for 24 h, as indicated. (*E* and *F*) Patient fibroblasts were challenged with TM as indicated for 24 h. The mRNA levels of IRE1 pathway downstream target gene, *ERdj4* (*E*), and PERK pathway downstream target gene, *CHOP* (*F*), were measured by real-time quantitative PCR and normalized to levels in untreated cells.

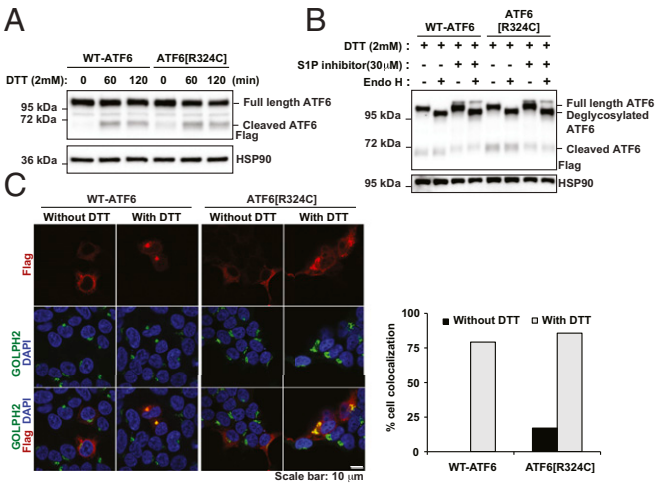

Fig. 5. Normal ER-to-Golgi trafficking of class 3 mutant, *ATF6*^{R324C} during ER stress. (*A*) Recombinant FLAG-tagged ATF6[R324C] was expressed in HEK293 cells for 20 h and then challenged with DTT, as indicated. ATF6 protein levels were detected by immunoblotting with anti-FLAG. (*B*) Recombinant FLAG-tagged wild-type ATF6 and ATF6[R324C] were expressed in HEK293 cells for 20 h and then challenged with DTT with or without S1P inhibitor, as indicated, for 90 min. Cell lysates were treated with Endo H, as indicated. ATF6 protein levels were detected by immunoblotting with anti-FLAG. (*C*) ATF6[Y567N] was expressed in HEK293 cells for 20 h and then challenged with 2 mM DTT for 40 min. The subcellular localization of ATF6 was visualized by immunofluorescence labeling and confocal microscopy by anti-FLAG antibody (shown in red). The Golgi apparatus was visualized by GOLPH2 immunostaining (shown in green). The nucleus was visualized by DAPI staining (shown in blue). The percentage of cells showing FLAG and GOLPH2 colocalization was quantified and shown in the graph. (Scale bar, 10 μm.)

protein folding chaperones and enzymes (7). If ER stress is not alleviated, cells ultimately undergo cell death (22, 23). We compared kinetics of cell death in patient fibroblasts expressing the class 1 and class 3 ATF6 mutants to see how the loss of ATF6 function affected survival during extended ER stress. In response to thapsigargin exposure, we observed significantly increased levels of the apoptosis marker, cleaved poly(ADP-ribose) polymerase (PARP), in *ATF6*$^{Y567N/Y567N}$ fibroblasts compared with heterozygous controls (Fig. 6*A*, cf. patient 3's fibroblasts with those of patients 1 and 2). Similarly, we observed increased levels of PARP cleavage in *ATF6*$^{R324C/R324C}$ fibroblasts compared with heterozygous parental control (Fig. 6*B*, cf. patients 2, 3, and 4 with patient 1's cells). These studies revealed that a physiologic consequence of the loss of ATF6 function caused by class 1 and class 3 ATF6 mutations was heightened cell death in response to ER stress.

Discussion

Our studies provide a framework for functional and pathomechanistic classification of *ATF6* mutations identified in achromatopsia (Fig. S1). Class 1 mutations affect the luminal domain of ATF6 and lead to loss of function. The pathomechanism underlying loss of function in class 1 ATF6 mutations is inefficient trafficking from ER to Golgi during ER stress, leading to poor production of the ATF6 transcriptional activator fragment (Fig. S1*A*). Class 2 mutations cluster near the transmembrane domain of ATF6. These mutations produce the entire cytosolic ATF6 fragment unbound to membrane and show fully intact ATF6 transcriptional activity (Fig. S1*A*). The class 2 *ATF6* transcripts all bear premature stop codons and are likely targets of nonsense-mediated mRNA decay machinery (1). Nonsense-mediated decay reduces mRNA transcript levels by ~50–85%, depending on tissue type and environmental factors (24). Therefore, whether class 2 mutations produce significant amounts of cytosolic ATF6 transcriptional activator fragment and show constitutive signaling in vivo requires further analysis in patients with these mutations. Class 3 mutations affect the cytosolic domain of ATF6 and lead to loss of function. The pathomechanism underlying loss of function in this class of mutations is deletion or mutation of the bZIP and/or transcriptional activator domain.

Do the mechanistic differences we identified between *ATF6* mutations lead to phenotypic differences? In particular, we found that a class 3 mutant had loss of ATF6 signaling plus significant impairment of the transcriptional output of IRE1 and PERK signaling (Fig. 4), whereas the class 1 mutant only showed minor impairment of the transcriptional output of IRE1 and PERK signaling (Fig. 1). One possibility is that up-regulation of ER stress genes, such as *ERdj4* and *CHOP*, requires the production of functional ATF6 cytosolic bZIP transcriptional activator domain. In this view, class 1 mutant ATF6 can still produce a functional cytosolic domain under ER stress, albeit with reduced efficiency. In contrast, class 3 mutant ATF6 produces a nonfunctional cytosolic domain. This could explain why the up-regulation of *ERdj4* and *CHOP* under ER stress is more severely impaired in class 3 mutant ATF6s. Our identification of distinct pathomechanisms of *ATF6* disease mutations enables prospective longitudinal study of retinal structure and phenotype to identify possible differences in achromatopsia disease phenotype and severity between carriers with different classes of *ATF6* mutations. Evaluation with adaptive optics and other retinal imaging modalities may reveal cone phenotype differences corresponding to different classes of *ATF6* mutations (25, 26).

What are the therapeutic implications of differences between *ATF6* mutations' mechanisms of pathology? Class 1 ATF6 mutants inefficiently traffic from ER to Golgi but have normal bZIP transcriptional activator domains. For this class of mutations, our findings indicate that therapeutic strategies should focus on improving protein trafficking out of the ER so the full-length ATF6 protein can be cleaved by the S1P and S2P Golgi-resident proteases. Once cleaved and separated from the defective luminal domain, the cytosolic ATF6 domain can engage in its normal transcriptional activator role. In contrast, the class 3 ATF6 mutants require a different therapeutic approach than class 1 trafficking mutants because class 3 mutants completely

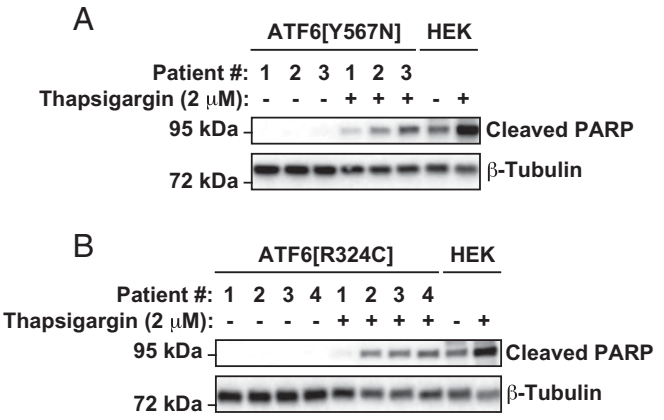

Fig. 6. Class 1 or class 3 mutant *ATF6* fibroblasts show increased susceptibility to ER stress-induced cell death. Class 1 *ATF6*$^{Y567N/+}$ or *ATF6*$^{Y567N/Y567N}$ human fibroblasts (*A*) and class 3 *ATF6*$^{R324C/+}$ or *ATF6*$^{R324C/R324C}$ human fibroblasts (*B*) were treated with thapsigargin at the indicated concentration for 3 or 6 d, respectively. Cleaved PARP protein was detected by immunoblotting. As a control for the position of cleaved PARP protein, HEK293 cells were treated with thapsigargin, and lysates were probed for PARP.

lack or bear defective bZIP/transcriptional activator domains. Gene therapy to introduce functional ATF6 bZIP transcriptional activator or gene editing to repair the primary *ATF6* nucleotide alterations may be potential therapeutic strategies for patients with these types of *ATF6* mutations.

Our current study highlights the surprisingly diverse molecular defects in the mechanism of ATF6 activation caused by achromatopsia-associated mutations. Patient fibroblasts with several of these mutations showed increased sensitivity to ER stress-induced cell death and damage. Diverse environmental insults have been found to trigger ER stress, including hypoxia, infection, inflammation, protein misfolding, and light damage (27–33). Exposure to these insults during retinal development may contribute to the cone dysfunction and vision loss that arises in children with mutations that compromise ATF6 function.

Materials and Methods

Cell Culture and Transfection. The maintenance and drug treatments of human primary fibroblast cells or HEK293 cells were described in detail in *SI Materials and Methods*. The generation of ATF6 mutant plasmids and the expression of these ATF6 mutants were described in detail in *SI Materials and Methods*.

Molecular Biology. Cells were lysed, and total RNA was collected using the RNeasy mini kit according to manufacturer's instructions (Qiagen). mRNA was reverse-transcribed, using the iScript cDNA Synthesis Kit (Bio-Rad). The methods for analyzing the level of *XBP1* mRNA splicing and the qPCR analysis of gene expression are described in detail in *SI Materials and Methods*.

Immunoblotting Analysis. Human fibroblasts or HEK293 cells expressing wild-type or mutant ATF6 were lysed in SDS lysis buffer [2% (g/vol) SDS, 62.5 mM Tris·HCl at pH 6.8, containing protease inhibitors (Sigma-Aldrich) and phosphatase inhibitor (Thermo Scientific)]. Protein concentrations of the total cell lysates were determined by bicinchoninic acid (BCA) protein assay (Pierce). Equal amounts of protein were loaded onto 10% or 4–15% Mini-PROTEAN TGX precast gels (Bio-Rad) and analyzed by Western blot, as described in *SI Materials and Methods*.

Endo H (New England Biolabs) digestion was performed on precleared total cell lysate for 1 h at 37 °C in the buffer supplied by the manufacturer. To preclear the cellular debris from the total lysate, cell lysate were spun at 21,900 × *g* at 4 °C for 1 h.

Immunofluorescence and Confocal Microscopy. Cells were grown on poly-D-lysine coated glass coverslips and transfected with wild-type ATF6 or ATF6 [Y567N]. For immunofluorescence analysis, cells were fixed for 20 min at room temperature in 4% paraformaldehyde in PBS at pH 7.4, washed briefly with PBS, and permeabilized with 0.1% Triton X-100 in PBS. Cells were then washed two times with 1% BSA in PBS and blocked with 5% (vol/vol) goat serum in 1% BSA/PBS for 20 min. The coverslips were then incubated at room temperature for 1 h with primary antibodies followed by secondary antibody incubation as described in *SI Materials and Methods*. The coverslips were mounted in ProLong Gold antifade reagent with DAPI (Invitrogen), and images were collected with an Olympus FluoView-1000 confocal microscope.

ACKNOWLEDGMENTS. We thank M. Wilkinson for helpful discussions on NMD and members of the J.H.L. laboratory for helpful review of the manuscript. S.H.T. is supported by the Barbara & Donald Jonas Laboratory of Regenerative Medicine; the Bernard & Shirlee Brown Glaucoma Laboratory; NIH Grants 5P30EY019007,R01EY018213, R01EY024698, R01EY026682, R21AG050437, and 5P30CA013696; the Research to Prevent Blindness Physician-Scientist Award; unrestricted funds from Research to Prevent Blindness; the Tistou and Charlotte Kerstan Foundation; the Crowley Family Fund; the Schneeweiss Stem Cell Fund; New York State (C029572); the Foundation Fighting Blindness New York Regional Research Center Grant (C-NY05-0705-0312); and the Gebroe Family Foundation. R.J.K. is supported by NIH Grants DK042394, DK103185, and DK088227. J.H.L. is supported by NIH Grants EY020846, NS088485, and U54OD020351, and VA Grant BX002284. The University of California, San Diego, School of Medicine Microscopy Core is supported by NIH Grants P30NS047101 and P30EY022589.

1. Kohl S, et al. (2015) Mutations in the unfolded protein response regulator ATF6 cause the cone dysfunction disorder achromatopsia. *Nat Genet* 47(7):757–765.
2. Ansar M, et al.; University of Washington Center for Mendelian Genomics (2015) Mutation of ATF6 causes autosomal recessive achromatopsia. *Hum Genet* 134(9): 941–950.
3. Xu M, et al. (2015) ATF6 Is Mutated in Early Onset Photoreceptor Degeneration With Macular Involvement. *Invest Ophthalmol Vis Sci* 56(6):3889–3895.
4. Haze K, Yoshida H, Yanagi H, Yura T, Mori K (1999) Mammalian transcription factor ATF6 is synthesized as a transmembrane protein and activated by proteolysis in response to endoplasmic reticulum stress. *Mol Biol Cell* 10(11):3787–3799.
5. Ye J, et al. (2000) ER stress induces cleavage of membrane-bound ATF6 by the same proteases that process SREBPs. *Mol Cell* 6(6):1355–1364.
6. Shen J, Chen X, Hendershot L, Prywes R (2002) ER stress regulation of ATF6 localization by dissociation of BiP/GRP78 binding and unmasking of Golgi localization signals. *Dev Cell* 3(1):99–111.
7. Wu J, et al. (2007) ATF6alpha optimizes long-term endoplasmic reticulum function to protect cells from chronic stress. *Dev Cell* 13(3):351–364.
8. Yamamoto K, et al. (2007) Transcriptional induction of mammalian ER quality control proteins is mediated by single or combined action of ATF6alpha and XBP1. *Dev Cell* 13(3):365–376.
9. Nadanaka S, Yoshida H, Kano F, Murata M, Mori K (2004) Activation of mammalian unfolded protein response is compatible with the quality control system operating in the endoplasmic reticulum. *Mol Biol Cell* 15(6):2537–2548.
10. Wang Y, et al. (2000) Activation of ATF6 and an ATF6 DNA binding site by the endoplasmic reticulum stress response. *J Biol Chem* 275(35):27013–27020.
11. Walter P, Ron D (2011) The unfolded protein response: from stress pathway to homeostatic regulation. *Science* 334(6059):1081–1086.
12. Wang M, Kaufman RJ (2016) Protein misfolding in the endoplasmic reticulum as a conduit to human disease. *Nature* 529(7586):326–335.
13. Calfon M, et al. (2002) IRE1 couples endoplasmic reticulum load to secretory capacity by processing the XBP-1 mRNA. *Nature* 415(6867):92–96.
14. Yoshida H, Matsui T, Yamamoto A, Okada T, Mori K (2001) XBP1 mRNA is induced by ATF6 and spliced by IRE1 in response to ER stress to produce a highly active transcription factor. *Cell* 107(7):881–891.
15. Shoulders MD, et al. (2013) Stress-independent activation of XBP1s and/or ATF6 reveals three functionally diverse ER proteostasis environments. *Cell Reports* 3(4): 1279–1292.
16. Hassler JR, et al. (2015) The IRE1α/XBP1s Pathway Is Essential for the Glucose Response and Protection of β Cells. *PLoS Biol* 13(10):e1002277.
17. Harding HP, Zhang Y, Bertolotti A, Zeng H, Ron D (2000) Perk is essential for translational regulation and cell survival during the unfolded protein response. *Mol Cell* 5(5):897–904.
18. Scheuner D, et al. (2001) Translational control is required for the unfolded protein response and in vivo glucose homeostasis. *Mol Cell* 7(6):1165–1176.
19. Harding HP, et al. (2000) Regulated translation initiation controls stress-induced gene expression in mammalian cells. *Mol Cell* 6(5):1099–1108.
20. Chiang WC, Hiramatsu N, Messah C, Kroeger H, Lin JH (2012) Selective activation of ATF6 and PERK endoplasmic reticulum stress signaling pathways prevent mutant rhodopsin accumulation. *Invest Ophthalmol Vis Sci* 53(11):7159–7166.
21. Bommiasamy H, et al. (2009) ATF6alpha induces XBP1-independent expansion of the endoplasmic reticulum. *J Cell Sci* 122(Pt 10):1626–1636.
22. Lin JH, et al. (2007) IRE1 signaling affects cell fate during the unfolded protein response. *Science* 318(5852):944–949.
23. Rutkowski DT, et al. (2006) Adaptation to ER stress is mediated by differential stabilities of pro-survival and pro-apoptotic mRNAs and proteins. *PLoS Biol* 4(11):e374.
24. Zetoune AB, et al. (2008) Comparison of nonsense-mediated mRNA decay efficiency in various murine tissues. *BMC Genet* 9:83.
25. Aboshiha J, et al. (2014) A prospective longitudinal study of retinal structure and function in achromatopsia. *Invest Ophthalmol Vis Sci* 55(9):5733–5743.
26. Genead MA, et al. (2011) Photoreceptor structure and function in patients with congenital achromatopsia. *Invest Ophthalmol Vis Sci* 52(10):7298–7308.
27. Kroeger H, et al. (2012) Induction of endoplasmic reticulum stress genes, BiP and chop, in genetic and environmental models of retinal degeneration. *Invest Ophthalmol Vis Sci* 53(12):7590–7599.
28. Yang LP, Wu LM, Guo XJ, Li Y, Tso MO (2008) Endoplasmic reticulum stress is activated in light-induced retinal degeneration. *J Neurosci Res* 86(4):910–919.
29. Nakanishi T, et al. (2013) Role of endoplasmic reticulum stress in light-induced photoreceptor degeneration in mice. *J Neurochem* 125(1):111–124.
30. Zhang SX, Ma JH, Bhatta M, Fliesler SJ, Wang JJ (2015) The unfolded protein response in retinal vascular diseases: implications and therapeutic potential beyond protein folding. *Prog Retin Eye Res* 45:111–131.
31. Zhang SX, Sanders E, Fliesler SJ, Wang JJ (2014) Endoplasmic reticulum stress and the unfolded protein responses in retinal degeneration. *Exp Eye Res* 125(0):30–40.
32. Alavi MV, et al. (2015) In Vivo Visualization of Endoplasmic Reticulum Stress in the Retina Using the ERAI Reporter Mouse. *Invest Ophthalmol Vis Sci* 56(11):6961–6970.
33. Chiang WC, et al. (2015) Robust Endoplasmic Reticulum-Associated Degradation of Rhodopsin Precedes Retinal Degeneration. *Mol Neurobiol* 52(1):679–695.